JAAS

Accepted Manuscript

This article can be cited before page numbers have been issued, to do this please use: A. Cañabate, E. García-Ruiz, M. Resano and J. Todoli Torro, *J. Anal. At. Spectrom.*, 2017, DOI: 10.1039/C7JA00210F.

View Article Online
DOI: 10.1039/C7JA00210F

Cerebrospinal fluid elemental analysis by using a total sample consumption system operated at high temperature adapted to inductively coupled plasma mass spectrometry

Águeda Cañabate,[1] Esperanza García-Ruiz,[2] Martín Resano,[2] José-Luis Todolí [1]

[1] Department of Analytical Chemistry, Nutrition and Food Sciences, University of Alicante, P.O. Box 99, 03080 Alicante, Spain.

[2] Department of Analytical Chemistry, Aragón Institute of Engineering Research (I3A), University of Zaragoza, Pedro Cerbuna 12, 50009, Zaragoza, Spain.

View Article Online
DOI: 10.1039/C7JA00210F

Abstract

A total consumption low sample introduction system has been applied for the first time to the multielemental analysis of non-diluted cerebrospinal fluids (CSF) by means of inductively coupled plasma mass spectrometry (ICP-MS). A 2.5 µL sample volume has been injected into an air carrier stream in agreement with the air-segmented injection principle. The sample plug has been turned out into an aerosol by means of a high efficiency nebulizer (HEN) and further introduced into the so-called high temperature torch integrated sample introduction system (hTISIS). A transient signal has been thus obtained. For spiked CSF real samples it has been verified that the higher the temperature, the greater the sensitivity. Under optimized conditions, the hTISIS provides peak areas around four times higher than those provided by the spectrometer default device (*i.e.*, a double pass spray chamber). Additional advantages incorporated by the former system include limits of detection up to 6 times lower and narrower peaks as compared to those reported for the double pass spray chamber. Furthermore, the use of the hTISIS is not detrimental from the point of view of neither oxide production nor doubly charged ion generation. Regarding the extent of non-spectral interferences caused by the CSF matrix, it has been verified that, with the hTISIS, recoveries for spiked real samples were close to 100% for a set of 14 different elements (V, Cr, Mn, Co, Ni, Cu, As, Se, Mo, Cd, Sb, Ba, Tl and Pb). Meanwhile, in segmented flow injection mode, the reference system provided recoveries from 200 to 500%, depending on the element and the sample, thus demonstrating the occurrence of matrix effects.

View Article Online
DOI: 10.1039/C7JA00210F

1. Introduction

Elemental analyses of clinical samples are of particular interest as they allow to determine the pathological conditions of patients.[1,2] Consequently, clinical laboratories are required to determine an increasing number of elements in body fluids.[3,4] Within this field, cerebrospinal fluid (CSF) is a sample of special relevance because the determination of trace elements in this fluid may provide information related with central nervous system (CNS) disorders. Acute brain affections such as stroke as well as chronic brain disorders such as Parkinson´s disease, Alzheimer´s disease and multiple sclerosis appear to cause changes in the concentration of trace elements in CSF.[5–10]

Basically, CSF is an excretion product of the choroid plexus of the CNS that fills the ventricles and the subarachnoid space of the brain and spinal column.[7–9] Table 1 lists the main components of CSF together with their approximate concentrations. This body fluid plays an important role in the homeostasis and metabolism of the CNS,[10,11] because it acts as a protection of brain structures against adverse effects of excess metal exposure and depletion of essential elements.[8] Additionally, CSF is directly connected to the extracellular space of the brain and facilitates molecular exchange.[7–9] Finally, this fluid protects the brain from physical shock.[7] The CSF composition is dependent upon extracellular fluids of brain and, hence, depends on changes of the elemental concentration in brain.

The determination of trace elements in CSF is a difficult task. On the one hand, sampling is normally performed by means of lumbar puncture and it is only permitted in cases of patients with confirmed neurological complaints. Therefore, the lack of real controls in terms of trace elements makes the detection of neurological disorders to

View Article Online
DOI: 10.1039/C7JA00210F

be a great challenge. On the other hand, the risk of contamination of CSF samples during sample collection, storage and treatment increases the sampling complexity.[8,12]

Trace elements have been determined in CSF through voltammetry[13], atomic absorption spectrometry (AAS),[9,14–19] inductively coupled plasma optical emission spectrometry (ICP-OES)[20–24] and inductively coupled plasma mass spectrometry (ICP-MS).[5,9,21–33] The last technique is the most suitable to perform this kind of analysis, due to its multi-element capability, high sensitivity and wide dynamic range.

However, ICP-MS elemental analysis of this human CSF samples is complex because of several reasons: i) first the concentration of the trace elements of interest is typically very low; ii) second, no CRMs are available;[8] iii) third, ICP-MS is prone to suffer from spectral as well as non-spectral interferences caused by the CSF matrix,[10,34] which may degrade accuracy.[12] Table 1 shows examples of possible spectral interferences when analysing CSF samples.[35] Fortunately, these unwanted phenomena can be minimized or even removed by using a reaction and/or collision cell in a quadrupole based ICP-MS instrument.[24,28,29,36] Alternatively, interferences are overcome by sample dilution, which degrades the sensitivity.[20]

In any case, it should be considered that the total CSF volume in adults is estimated to be about 100-150 mL. Therefore, a small portion of this body fluid must be collected in order to prevent severe headaches. It is thus compulsory to devise methods able to consume an amount of sample as low as possible.[10]

In this sense, use of total sample consumption systems can be advantageous. The so-called Torch Integrated Sample Introduction System working at high temperatures (hTISIS) consists of a micronebulizer associated to a low inner volume

View Article Online
DOI: 10.1039/C7JA00210F

(*c.a.*, 9 cm^3) single pass spray chamber.[37,38] The hTISIS is perfectly indicated to work at low liquid flow rates and under air-segmented flow injection mode.[39–41] The latter injection methodology shows several advantages, such as a low sample consumption volume, an increased sensitivity and shortened wash-out times, with respect to continuous sample aspiration mode. This injection mode has been recently combined with the hTISIS for whole blood analysis *via* ICP-MS.[42] By introducing just 2 – 5 μL of properly diluted sample into the air carrier stream, sensitivities provided by the hTISIS were up to four times higher than those afforded by a conventional liquid sample introduction setup. More importantly, since for the hTISIS the analyte transport efficiency became 100% regardless of the sample matrix, the interferences associated to the sample introduction system were removed thus making it possible to perform calibration with plain water standards.

The aim of the present study was thus to perform, for the first time, non-diluted CSF analysis through hTISIS-ICP-MS. To achieve this goal, the chamber temperature was optimized for spiked real samples. The results were compared against those provided by a double pass spray chamber. Due to the lack of certified materials, CSF samples from human subjects were spiked and recoveries were measured. Further validation studies were undertaken and the trace elements concentrations found by applying two different quantification methodologies (*i.e.*, single standard addition and external calibration with plain water standards) were compared using the two sample introduction systems tested in the present work. In the former case, only two solutions were analyzed: a standard corresponding to the spiked sample and the sample itself. The developed method was finally applied to the analysis of CSF real samples.

View Article Online
DOI: 10.1039/C7JA00210F

View Article Online
DOI: 10.1039/C7JA00210F

2. Experimental

2.1 Chemicals and samples

Standards and samples were prepared in 1% nitric acid (HNO_3 65% Suprapur®, Merck, Darmstadt, Germany) whereas ultra-pure water was obtained from a Milli-Q system (Merck).

EPA Method 200.8-1 stock solutions (High-Purity Standards, Charleston, USA), containing 10 μg element mL^{-1} were used to prepare the standards. Besides, a single element stock solution containing 1000 mg Ce L^{-1} (Merck) was used to perform studies related with oxide production and double charge ratios.

Samples from human donors were provided by the Hospital Universitario Miguel Servet, Zaragoza and the principles outlined in the declaration of Helsinki for all human investigations were followed. In addition, informed consent was obtained from all the participants involved.

In order to perform the sampling procedure, lumbar punctures were done with the patients in a lateral recumbent knee flexed to chest position. The total extracted fluid volume per patient ranged between 2 and 4 mL. Blood polluted spinal punctures were excluded from the study. The CSF samples were frozen at -30°C and protected from light exposure until analysis. Non-diluted samples were directly analyzed.

2.2 Instrumentation

An Agilent 7700x ICP-MS (Santa Clara, USA) equipped with a 12 MHz octopole ORS cell was used throughout. This instrument is equipped with a High Matrix Introduction

View Article Online
DOI: 10.1039/C7JA00210F

(HMI) accessory that increases the tolerance to salty matrices. Table 2 summarizes the ICP-MS operating conditions. The hTISIS was equipped with a High Efficiency Nebulizer (HEN, Meinhard Glass Products, Santa Ana, USA). Besides, a 110 cm^3 inner volume double pass spray chamber set at a temperature of 2°C was used as the reference chamber for comparative studies.

Samples were delivered to the nebulizer by means of the spectrometer peristaltic pump using 0.19 mm i.d. flared end PVC-based tubing (Glass Expansion, Melbourne, Australia). Air was continuously aspirated and, at a given time, 2.5 µL of either samples or standards, measured with an automatic pipette (Eppendorf, Hamburg, Germany), were injected into the air stream by adapting the nozzle to the flared end tubing. The solution was driven towards the nebulizer, thus giving rise to a transient signal.

3. Results and discussion

In order to mitigate interferences, CFS samples are usually diluted before their analysis *via* ICP-MS. [4,8,20-32] The dilution factor goes from 1:4 to 1:50, depending on the element to be quantified. According to some studies, a CFS digestion should be performed in order to decompose the organic CSF concomitants.[27,32] Obviously, these procedures lead to a degradation in the detection power of the methodology. In the present work, non-diluted samples were directly analyzed. Interestingly, no salty deposits were observed on the ICP-MS interface sampling cone. The main reasons to account for this observation were based on the facts that a small sample volume was injected into the system and the spectrometer used was equipped with an aerosol phase dilution device (*i.e.*, the so-called High Matrix Introduction, HMI). This accessory involves the decrease

View Article Online
DOI: 10.1039/C7JA00210F

in the nebulizer gas flow rate and the introduction of an additional argon stream at the exit of the spray chamber so as to keep the total central gas flow rate at a suitable level. The use of the HMI stream caused the aerosol plug gas phase dilution at the exit of the chamber. Therefore, the mass of matrix reaching the plasma per unit of time decreased.

3.1. Optimization of the chamber temperature and comparison of the hTISIS with the double pass spray chamber

In the case of the hTISIS, the aerosol heating temperature was a critical variable affecting the sensitivity of the CSF determination. Fig. 1 shows the variation of peak area, for a spiked CSF sample, versus the hTISIS temperature. For the sake of simplicity, the peak areas were normalized to those obtained when the conventional sample introduction system was operated. It was clearly noticed that, the higher the temperature, the stronger the relative peak area. This was due to the increase in the extent of aerosol evaporation inside the hTISIS chamber with the concomitant growth in analyte transport efficiency. At 400°C, the sensitivity either reached a plateau or slightly decreased thus suggesting that the analyte transport efficiency was close to 100% at 200°C. For Se, As, Sb, Tl and Pb, the peak area was lower at 400°C than at 200°C. This fact could be attributed to a greater dispersion of ions in the plasma thus leading to a decrease in the sampling efficiency. According to this idea, a fraction of Se, As, Sb, Tl and Pb would evaporate inside the hTISIS. This explanation was supported by the fact that either these elements or their oxides had lower melting and/or boiling points than the remaining analytes (or their oxides). As it was observed for blood

View Article Online
DOI: 10.1039/C7JA00210F

samples,[42] average peak areas found for the hTISIS were around four times higher than those measured for the double pass spray chamber.

In these studies, it was confirmed that the hTISIS working at 200°C provided narrower peaks than the conventional spray chamber (Fig. 2). In fact, wash out times defined as the time required for the signal to drop down to 1% of its maximum value were about 30 and 9 seconds for the double pass spray chamber and the hTISIS, respectively. The reasons that can explain these differences are: *(i)* the inner volume of the hTISIS (*i.e.*, 9 cm^3) was roughly one order of magnitude lower than that for the double pass spray chamber (*i.e.*, 110 cm^3); and, *(ii)* because the totality of the solution evaporated inside the spray chamber, no re-nebulization processes were produced from the chamber inner walls.

3.2. Validation of the proposed methodology

It was verified that the hTISIS did not compromise the repeatability of the results. Signal stability was evaluated by calculating the peak area RSD of five consecutive sample injections (Fig. 3). RSD average values for all elements were 9.0 ± 1.4 for the double pass spray chamber and 6.7 ± 2.4 for the hTISIS at 200°C. An ANOVA test was applied to both RSD datasets and the results revealed that there were statistically significant differences for the two sample introduction systems and the fourteen isotopes considered (t_{cal} = 3.11; t_{tab} = 2.08; α = 0.05). The data suggested that the hTISIS provided RSDs values similar to or lower than those calculated for the reference spray chamber.

View Article Online
DOI: 10.1039/C7JA00210F

Limits of detection were calculated according to the $3s_b$ criterion, where s_b was the standard deviation of a series of five consecutive blank injections. Meanwhile, quantification limits were calculated according to the $10s_b$ criterion. In both cases, sensitivity was obtained as the average peak area of a 10 μg L^{-1} standard divided by its concentration. Table 3 summarizes the results. It was observed that the hTISIS working at 200°C provided LODs of approximately 1 μg L^{-1} or lower (except for Se), without the concourse of any collision or reaction gas, which are up to 6 times lower than those provided by the double pass spray chamber.

3.2. Oxides and doubly charged ions

As expected, the oxide ratio increased with the hTISIS temperature because of the rise in the mass of solvent vapor reaching the plasma (Fig. 4). Nevertheless, the oxide levels remained low. It was found that this parameter ranged from 0.6 to 1.1 % as the hTISIS temperature was increased from room temperature to 400°C. Note that the oxide ratio for the double pass spray chamber took a value close to 0.5%. Globally speaking, these results ensured a low contribution of these species to spectral interferences. When considering doubly charged ions (Fig. 4) similar Ce^{++}/Ce^{+} ratios were found for the double pass spray chamber and hTISIS at different temperatures. In other words, the plasma was not thermally degraded when employing the latter sample introduction system. The main reason for this observation lied in the extremely low sample volume analyzed.

3.3. Non-spectral interferences

View Article Online
DOI: 10.1039/C7JA00210F

In order to evaluate the extent of the matrix effects CSF direct analyses were carried out. The elemental concentrations were obtained by two calibration methods: *(i)* external calibration using plain water standards; and, *(ii)* single standard addition, which is supposed to compensate for non-spectral interferences. In the case of the latter method, the sample was spiked with a 20 μg L^{-1} multielemental concentration whereas the non-spiked sample was taken as the blank. The analytical (C_a) concentration was determined by applying the following mathematical relationship:

$$C_a = \frac{Sa\ C_s}{S_s} \qquad (1)$$

where S_a and S_s corresponded to the signal provided by the non-spiked and the spiked sample, respectively, and C_s was the added analyte concentration (*i.e.*, 20 μg L^{-1}). Afterwards, a concentrations ratio (C_R) was calculated according to:

$$C_R = \frac{C_{Single\ standard\ addition}}{C_{external\ calibration}} \qquad (2)$$

In the case of the double pass spray chamber (Fig. 5.a), it was found that, for a set of five CSF real samples, the concentration resulting from applying the single standard addition procedure was 2.5 to 5 times lower than that encountered when quantification was done using external calibration (*i.e.*, C_R from 0.4 to 0.2). Surprisingly, in the case of copper, C_R was close to 1. It was later verified that copper was highly sensitive to changes in the matrix composition. Most important, for the hTISIS (Fig. 5.b), the ratios for all elements were generally close to one. This fact suggested that matrix effects were alleviated when using the total sample consumption system

View Article Online
DOI: 10.1039/C7JA00210F

Due to the lack of certified CSF reference materials (CRMs), recovery tests were performed with both sample introduction systems. Therefore, CSF real samples were spiked with 20 µg L^{-1} multielemental solution to evaluate the extent of matrix effects. The resulting solutions were analyzed by applying external calibration with ultra-pure water standards. The recoveries are summarized in Fig. 6. It is interesting to notice that the appearance of matrix effects and high LOQs (see Table 3) could be the main reasons to account for the high recoveries found when the double pass spray chamber was used (Fig. 6a). However, recoveries close to 100% were obtained when the hTISIS was operated at 200°C (Fig. 6b). These results confirmed that non spectral interferences caused by complex matrices were minimized when using this total sample consumption device.

3.4. Analysis of real samples

The elemental concentrations found for five samples by using the two calibration methods are gathered in Table 4 for the hTISIS operated at 200°C. It may be observed that, as expected from Fig. 5, for all the tested samples the found concentrations were similar irrespectively of the calibration method utilized. Only in the case of copper for sample D, the two assayed methods provided significantly different concentrations. As previously mentioned, copper demonstrated to be the element most sensitive to matrix effects. Therefore, it was possible to perform elemental CSF analysis by merely using the hTISIS at 200°C and external calibration with plain water standards.

A set of additional 6 samples were directly analyzed using the hTISIS (Table 5). The data were obtained by applying both external calibration and single standard

View Article Online
DOI: 10.1039/C7JA00210F

addition (data not shown). An aqueous standard was analysed every ten samples to verify the absence of signal drift. Again, concentrations were similar for both calibration approaches. By examining the data presented in Tables 4 and 5, it emerged that significant differences were found among samples when considering elements having a demonstrated influence in neurological process.[5] Thus, for instance, samples F, G and I (Table 5) had significantly lower contents of Mn than the remaining specimens (see Tables 4 and 5). Moreover, copper in samples I and K was present at much higher levels than for the remaining CSF samples. Samples J and K, in turn, were significantly enriched in cadmium and lead (Table 5). All these observations can be highly significant in the context of a clinical and deeper study aimed at the establishment of correlations between the elemental content and the incidence of neurological disorders.

4. Conclusions

The hTISIS in combination with an air segmented methodology is highly indicated to perform accurate CSF elemental analysis *via* ICP-MS. Compared with a conventional sample introduction system, the main advantages of the hTISIS are: *(i)* an increase in sensitivity and a decrease in limits of detection, caused by a combination of an increased analyte transport efficiency and a decreased peak dispersion in the chamber; and, *(ii)* a virtual removal of matrix effects, likely due to the increase in analyte transport efficiency up to values close to 100%, regardless of the sample composition. Taking into account the methods previously described in the literature, additional

View Article Online
DOI: 10.1039/C7JA00210F

advantages are reported in the present work such as a remarkable decrease in the amount of sample required to perform the analysis. In addition, as the sample should be neither diluted nor digested, the precision of the method was very good. According to our estimations, it is possible to perform 120 – 150 analysis h^{-1} with no salt deposits formation at the sampler cone of the ICP-MS interface.

Analyte concentrations similar to those previously reported in the literature for CSF human samples were encountered when using hTISIS-ICP-MS.[5,19–21,24,29,31–33] The present study could be of great importance for further understanding of the relationships between neurological diseases and elemental concentration in CSF samples. On this subject, there are two main limitations: establishing reliable values for the metal concentrations of the control population, and the analysis of a number of samples (patients) high enough to draw unequivocally useful conclusions on this subject.

View Article Online
DOI: 10.1039/C7JA00210F

Acknowledgements

The authors acknowledge the funding from CTQ2015-64684-P (MINECO/FEDER) and from the Aragón Government (Fondo Europeo de Desarrollo Regional). The authors would also like to thank to Geoff Coleman for the loan of the glass pneumatic concentric nebulizer and Dr. L. Rello from the Hospital Universitario Miguel Servet for the cooperation and for providing the samples. Águeda C. would like to thank the Vice-Presidency for Research of the University of Alicante (ref. UAFPU2015-5990), and the Generalitat Valenciana, Spain (ref. ACIF/2016/042) for the pre-doctoral grants.

View Article Online
DOI: 10.1039/C7JA00210F

References

1 I. Rodushkin, E. Engström and D. C. Baxter, *Anal. Bioanal. Chem.*, 2013, **405**, 2785–2797.

2 M. Krachler and K. J. Irgolic, *J. Trace Elem. Med. Biol.*, 1999, **13**, 157–169.

3 M. A. Vaughan, A. D. Baines and D. M. Templeton, *Clin. Chem.*, 1991, **37**, 210–5.

4 P. Heitland and H. D. Köster, in *Analytical Techniques for Clinical Chemistry. Methods and Applications*, eds. S. Caroli and G. Zaray, John Wiley & Sons, Inc., USA, 2012, pp. 367–395.

5 R. Mandal, A. C. Guo, K. K. Chaudhary, P. Liu, F. S. Yallou, E. Dong, F. Aziat and D. S. Wishart, *Genome Med.*, 2012, **4**, 1–11.

6 A. Takeda, *J. Heal. Sci.*, 2004, **50**, 429–442.

7 D. S. Wishart, M. J. Lewis, J. A. Morrissey, M. D. Flegel, K. Jeroncic, Y. Xiong, D. Cheng, R. Eisner, B. Gautam, D. Tzur, S. Sawhney, F. Bamforth, R. Greiner and L. Li, *J. Chromatogr. B*, 2008, **871**, 164–173.

8 B. Michalke and V. Nischwitz, *Anal. Chim. Acta*, 2010, **682**, 23–36.

9 B. Michalke, P. Grill and A. Berthele, *J. Trace Elem. Med. Biol.*, 2009, **23**, 243–250.

10 L. Sakka, G. Coll and J. Chazal, *Eur. Ann. Otorhinolaryngol. Head Neck Dis.*, 2011, **128**, 309–316.

11 Cerebrospinal Fluid Analysis, *http://emedicine.medscape.com/article/2093316-overview*, (accessed June 2017).

12 B. Bocca, G. Forte, F. Petrucci, O. Senofonte, N. Violante and A. Alimonti, *Ann.*

View Article Online
DOI: 10.1039/C7JA00210F

Ist. Super. Sanita, 2005, **41**, 165–170.

13 K. E. Johnson and R. G. Treble, 1993, **71**, 824–826.

14 G. F. Van Landeghem, P. C. D´Haese, L. V. Lamberts, J. D. Barata and M. E. De Broe, *Nephrol. Dial. Transplant.*, 1997, **12**, 1692–1698.

15 M. V. Aguilar, F. J. Jiménez-Jiménez, J. A. Molina, I. Meseguer, C. J. Mateos-Vega, M. J. González-Muñoz, F. De Bustos, C. Gómez-Escalonilla, M. Ortí-Pareja, M. Zurdo and M. C. Martínez-Para, *J. Neural Transm.*, 1998, **105**, 1245–1251.

16 I. Meseguer, J. A. Molina, F. J. Jiménez-Jiménez, M. V Aguilar, C. J. Mateos-Vega, M. J. González-Muñoz, F. De Bustos, M. Ortí-Pareja, M. Zurdo, A. Berbel, E. Barrios and M. C. Martínez-Para, *J Neural Transm*, 1999, **106**, 309–315.

17 J. L. Burguera, M. Burguera and O. M. Alarcon, *J. Anal. At. Spectrom.*, 1986, **1**, 79–83.

18 E. M. González-Romarís, I. Idoate-Cervantes, J. M. González-López and J. F. Escanero-Marcén, *J. Trace Elem. Med. Biol.*, 2011, **25**, S45–S49.

19 J. A. Molina, F. J. Jiménez-Jiménez, M. V Aguilar, I. Meseguer, C. J. Mateos-Vega, M. J. González-Muñoz, F. de Bustos, J. Porta, M. Ortí-Pareja, M. Zurdo, E. Barrios and M. C. Martínez-Para, *J. Neural Transm.*, 1998, **105**, 479–488.

20 G. Forte, B. Bocca, O. Senofonte, F. Petrucci, L. Brusa, P. Stanzione, S. Zannino, N. Violante, A. Alimonti and G. Sancesario, *J. Neural Transm.*, 2004, **111**, 1031–1040.

21 A. Alimonti, B. Bocca, A. Pino, F. Ruggieri, G. Forte and G. Sancesario, *J. Trace Elem. Med. Biol.*, 2007, **21**, 234–241.

22 M. Korvela, A. L. Lind, M. Wetterhall, T. Gordh, M. Andersson and J. Pettersson, *J. Trace Elem. Med. Biol.*, 2016, **37**, 1–7.

View Article Online
DOI: 10.1039/C7JA00210F

23 B. Bocca, A. Alimonti, O. Senofonte, A. Pino, N. Violante, F. Petrucci, G. Sancesario and G. Forte, *J. Neurol. Sci.*, 2006, **248**, 23–30.

24 V. Nischwitz, A. Berthele and B. Michalke, *Anal. Chim. Acta*, 2008, **627**, 258–269.

25 F. Boström, O. Hansson, L. Gerhardsson, T. Lundh, L. Minthon, E. Stomrud, H. Zetterberg and E. Londos, *Neurobiol. Aging*, 2009, **30**, 1265–1271.

26 B. Michalke, S. Halbach, A. Berthele, P. Mistriotis and M. Ochsenkühn-Petropoulou, *J. Anal. At. Spectrom.*, 2007, **22**, 267–272.

27 B. Bocca, A. Alimonti, F. Petrucci, N. Violante, G. Sancesario, G. Forte and O. Senofonte, *Spectrochim. Acta Part B*, 2004, **59**, 559–566.

28 K. Gellein, J. H. Skogholt, J. Aaseth, G. B. Thoresen, S. Lierhagen, E. Steinnes, T. Syversen and T. P. Flaten, *J. Neurol. Sci.*, 2008, **266**, 70–78.

29 V. Nischwitz, A. Berthele and B. Michalke, *J. Anal. At. Spectrom.*, 2010, **25**, 1130–1137.

30 I. Hozumi, T. Hasegawa, A. Honda, K. Ozawa, Y. Hayashi, K. Hashimoto, M. Yamada, A. Koumura, T. Sakurai, A. Kimura, Y. Tanaka, M. Satoh and T. Inuzuka, *J. Neurol. Sci.*, 2011, **303**, 95–99.

31 P. M. Roos, O. Vesterberg, T. Syversen, T. P. Flaten and M. Nordberg, *Biol. Trace Elem. Res.*, 2013, **151**, 159–170.

32 K. Gellein, P. M. Roos, L. Evje, O. Vesterberg, T. P. Flaten, M. Nordberg and T. Syversen, *Brain Res.*, 2007, **1174**, 136–142.

33 I. Hozumi, A. Kohmura, A. Kimura, T. Hasegawa, A. Honda, Y. Hayashi, K. Hashimoto, M. Yamada, T. Sakurai, Y. Tanaka, M. Satoh and T. Inuzuka, *Case Rep. Neurol.*, 2010, **2**, 46–51.

34 R. Spector, S. R. Snodgrass and C. E. Johanson, *Exp. Neurol.*, 2015, **273**, 57–68.

View Article Online
DOI: 10.1039/C7JA00210F

35 T. W. May and R. H. Wiedmeyer, *At. Spectrosc.*, 1998, **19**, 150–155.

36 I. Rodushkin, P. Nordlund, E. Engström and D. C. Baxter, *J. Anal. At. Spectrom.*, 2005, **20**, 1250–1255.

37 J. L. Todolí and J. M. Mermet, *J. Anal. At. Spectrom.*, 2002, **17**, 345–351.

38 F. Ardini, M. Grotti, R. Sánchez and J. L. Todolí, *J. Anal. At. Spectrom.*, 2012, **27**, 1400–1404.

39 D. Beauchemin, *Analyst*, 1993, **118**, 815–819.

40 J. M. Craig and D. Beauchemin, *Analyst*, 1994, **119**, 1677–1682.

41 J. M. Craig and D. Beauchemin, *J. Anal. At. Spectrom.*, 1994, **9**, 1341–1349.

42 Á. Cañabate, E. García-Ruiz, M. Resano and J. L. Todolí, *J. Anal. At. Spectrom.*, 2017, **32**, 78–87.

View Article Online
DOI: 10.1039/C7JA00210F

Table 1 Human CSF main components and examples of spectral ICP-MS interferences caused by the matrix.

Species		Approximate level*	Interfering ions in ICP-MS#
Electrolytes	Na^+	3,000 μg mL^{-1}	$^{40}Ar^{23}Na^+$ on ^{63}Cu $^{23}Na^{32}S^+$ on ^{55}Mn $^{23}Na^{37}Cl^+$ on ^{60}Ni
	K^+	100 μg mL^{-1}	$^{39}K^{16}O^+$ on ^{55}Mn
	Ca^{2+}	50 μg mL^{-1}	$^{23}Na^{40}Ca^+$ on ^{63}Cu $^{40}Ca^{16}O^1H^+$ on ^{65}Cu $^{40}Ca^{16}O^+$ on ^{56}Fe $^{40}Ca^{18}O^+$ on ^{58}Ni
	Cl^-	4,000 μg mL^{-1}	$^{40}Ar^{35}Cl^+$ on ^{75}As $^{37}Cl^{15}O^+$ on ^{53}Cr $^{23}Na^{35}Cl^+$ on ^{60}Ni $^{35}Cl^{16}O^+$ on ^{51}V
	HCO_3^-	1,200 μg mL^{-1}	
Glucose		600 μg mL^{-1}	
Vitamins	Vitamin C, folate, thiamine monophosphate, pyridoxal phosphate	---------	$^{12}C_2^+$ on ^{24}Mg $^{12}C^{15}N^+$ on ^{27}Al $^{14}N_2^+$, $^{12}C^{16}O^+$ on ^{28}Si $^{40}Ar^{12}C^+$ on ^{52}Cr $^{32}S^{16}O_2^+$ on ^{64}Zn
	Paradoxical transport (riboflavin, nucleosides and Cu+)		
Proteins and peptides	Leptin, prolactin and IGF-1	200 μg mL^{-1}	
	Transthyretin, IGF-2, BDNF		
	Albumin and immunoglobulins		
Other growth factors and brain maintenance substances	90 species RNA not present in plasma		

* Taken from refs. 10, 11, 34.

Information contained in ref. 35.

View Article Online
DOI: 10.1039/C7JA00210F

Table 2 ICP-MS operating conditions

Nebulizer gas flow rate	0.5 L min^{-1}
HMI flow rate	0.56 L min^{-1}
RF power	1,600 W
Plasma gas flow rate	15 L min^{-1}
Auxiliary gas flow rate	0.90 L min^{-1}
Dwell time	20 ms
Settling time	40 ms
Total acquisition time	600 s
Cell gas flow rate (He)	4.3 mL min^{-1}

View Article Online
DOI: 10.1039/C7JA00210F

Table 3 Limits of detection and quantification (µg L^{-1}) obtained under segmented-flow injection mode for different elements with the double pass spray chamber and hTISIS at 200°C.

	Double pass		hTISIS 200°C	
	LOD	LOQ	LOD	LOQ
^{51}V	0.8	2.7	0.2	0.5
^{52}Cr	1.2	4.1	0.8	2.5
^{55}Mn	1.3	4.3	0.6	2.0
^{59}Co	1.4	4.8	1.1	3.7
^{60}Ni	3.0	10.1	0.5	1.7
^{65}Cu	1.2	4.0	1.1	3.7
^{75}As	1.0	3.2	0.6	1.9
^{78}Se	8.4	28.0	3.8	12.7
^{95}Mo	2.5	8.3	0.6	1.9
^{111}Cd	0.8	2.6	0.2	0.5
^{121}Sb	0.7	2.2	0.1	0.4
^{137}Ba	1.0	3.4	0.4	1.4
^{205}Tl	1.1	3.6	0.7	2.2
^{208}Pb	6.8	22.7	1.1	3.7

Table 4 Elemental concentrations (in μg L^{-1}) found for five real samples of CSF by both calibration methods using hTISIS at 200°C[a]

	Sample A		Sample B		Sample C		Sample D		Sample E	
	External Calibration	Single standard addition	External Calibration	Single standard addition	External Calibration	Single standard addition	External Calibration	Single standard addition	External Calibration	Single standard addition
^{51}V	5.6 ± 0.2	6.3 ± 0.6	4.1 ± 0.2	4.1 ± 0.8	1.56 ± 0.05	1.49 ± 0.12	4.11 ± 0.17	4.5 ± 0.5	3.20 ± 0.07	3.50 ± 0.13
^{52}Cr	6.1 ± 0.4	6.6 ± 1.3	4.5 ± 0.3	4.9 ± 1.2	5.0 ± 0.3	5.1 ± 1.4	4.9 ± 0.3	5.5 ± 0.7	5.9 ± 0.3	7.4 ± 1.1
^{55}Mn	6.0 ± 0.3	6.8 ± 0.7	7.5 ± 0.6	6.2 ± 1.4	6.4 ± 0.3	6.0 ± 0.5	11.6 ± 0.4	13.0 ± 1.2	7.5 ± 0.4	7.0 ± 0.8
^{59}Co	3.1 ± 0.2*	3.5 ± 0.7*	2.92 ± 0.11*	3.3 ± 0.6*	5.6 ± 0.5	5.2 ± 0.9	3.3 ± 0.2*	3.9 ± 0.8*	11.7 ± 1.7	9.8 ± 0.2
^{60}Ni	5.7 ± 0.6	7.2 ± 1.1	4.3 ± 0.3	6.8 ± 0.8	19 ± 3	22 ± 6	10.9 ± 0.6	9.8 ± 1.3	30 ± 4	32 ± 9
^{65}Cu	25 ± 6	18 ± 4	21 ± 5	36 ± 6	28.6 ± 1.4	29.9 ± 1.2	9.4 ± 1.1	28 ± 7	10.2 ± 1.9	9.1 ± 1.2
^{75}As	0.93 ± 0.05*	0.86 ± 0.13*	0.81 ± 0.03*	0.79 ± 0.09*	1.01 ± 0.05*	0.93 ± 0.12*	1.12 ± 0.05*	1.23 ± 0.15*	1.14 ± 0.08*	1.3 ± 0.2*
^{78}Se	9.4 ± 0.8*	7.7 ± 1.5*	10.3 ± 0.6*	11.2 ± 1.1*	9.0 ± 1.8*	6.6 ± 1.1*	7.1 ± 1.7*	8.6 ± 1.3*	7.7 ± 0.9*	7 ± 2*
^{95}Mo	1.56 ± 0.05*	1.54 ± 0.13*	1.37 ± 0.06*	1.6 ± 0.3*	1.90 ± 0.15	2.1 ± 0.5	1.79 ± 0.11*	2.1 ± 0.3	1.52 ± 0.13*	1.8 ± 0.4*
^{111}Cd	6.9 ± 0.6	8 ± 2	3.7 ± 0.3	4.0 ± 1.5	5.95 ± 0.17	5.5 ± 0.4	4.05 ± 0.18	4.9 ± 0.5	2.00 ± 0.10	2.0 ± 0.2
^{121}Sb	1.9 ± 0.3	1.5 ± 0.3	1.12 ± 0.08	1.1 ± 0.3	1.06 ± 0.05	0.98 ± 0.12	1.55 ± 0.07	1.7 ± 0.2	1.19 ± 0.06	1.39 ± 0.19
^{137}Ba	9.4 ± 0.4	10.0 ± 1.2	8.7 ± 0.2	8.8 ± 0.2	5.19 ± 0.14	4.3 ± 0.3	6.7 ± 0.4	7.2 ± 1.3	6.6. ± 0.6	7.3 ± 1.6
^{205}Tl	9.3 ± 0.7	12 ± 2	2.53 ± 0.16	2.7 ± 0.5	2.50 ± 0.12	2.6 ± 0.3	4.7 ± 0.3	5.8 ± 0.4	3.1 ± 0.3	3.0 ± 0.8
^{208}Pb	10.0 ± 0.4	13.0 ± 1.6	10.1 ± 0.5	14 ± 3	7.4 ± 0.3	6.4 ± 0.8	7.0 ± 0.3	8.1 ± 0.8	2.7 ± 0.5*	3.5 ± 0.9*

* LOD < x ≤ LOQ

[a] Confidence intervals were calculated as $\pm(t\ s)/(N)^{1/2}$ being N=5.

View Article Online
DOI: 10.1039/C7JA00210F

Table 5. Elemental concentrations (in μg L^{-1}) found for six CSF real samples obtained using hTISIS at 200°C with external calibration[a]

	Sample F	Sample G	Sample H	Sample I	Sample J	Sample K
^{51}V	0.76 ± 0.05	1.72 ± 0.09	1.23 ± 0.06	1.96 ± 0.19	2.12 ± 0.09	1.61 ± 0.15
^{52}Cr	2.50 ± 0.14	2.42 ± 0.16*	3.04 ± 0.16	3.3 ± 0.3	2.7 ± 0.2	2.19 ± 0.12*
^{55}Mn	2.32 ± 0.10	2.29 ± 0.13	4.50 ± 0.16	2.4 ± 0.2	9.6 ± 0.9	5.0 ± 0.3
^{59}Co	< 1.1	< 1.1	< 1.1	< 1.1	1.7 ± 0.3	0.69 ± 0.15
^{60}Ni	2.7 ± 0.4	1.4 ± 0.2	7.0 ± 1.1	7.1 ± 0.9	7.6 ± 0.5	3.1 ± 0.2
^{65}Cu	11.2 ± 0.6	19.2 ± 0.7	17 ± 6	100 ± 10	37 ± 6	83 ± 3
^{75}As	1.62 ± 0.17*	2.42 ± 0.13	3.2 ± 0.2	3.3 ± 0.2	2.11 ± 0.14	2.31 ± 0.16
^{78}Se	4.2 ± 0.3*	4.9 ± 0.3*	5.3 ± 0.7*	6.3 ± 0.6*	5.2 ± 0.4*	6.0 ± 0.5*
^{95}Mo	1.25 ± 0.04	< 0.6	< 0.6	1.01 ± 0.08	0.39 ± 0.07	0.37 ± 0.02
^{111}Cd	2.2 ± 0.8	0.420 ± 0.017*	1.34 ± 0.14	0.38 ± 0.08	9.9 ± 0.6	7.1 ± 0.5
^{121}Sb	0.79 ± 0.04	1.38 ± 0.05	1.50 ± 0.10	2.28 ± 0.15	1.31 ± 0.12	1.5 ± 0.06
^{137}Ba	0.63 ± 0.10*	1.17 ± 0.11*	1.61 ± 0.12	1.30 ± 0.13*	9.5 ± 1.0	4.4 ± 0.4
^{205}Tl	0.79 ± 0.07*	1.23 ± 0.14*	2.0 ± 0.2*	2.1 ± 0.2*	2.4 ± 0.2*	1.56 ± 0.13*
^{208}Pb	< 1.1	< 1.1	< 1.1	< 1.1	4.6 ± 0.3	2.80 ± 0.16

* LOD < x ≤ LOQ

[a] Confidence intervals were calculated as ±(t s)/$(N)^{1/2}$ being N=5.

View Article Online
DOI: 10.1039/C7JA00210F

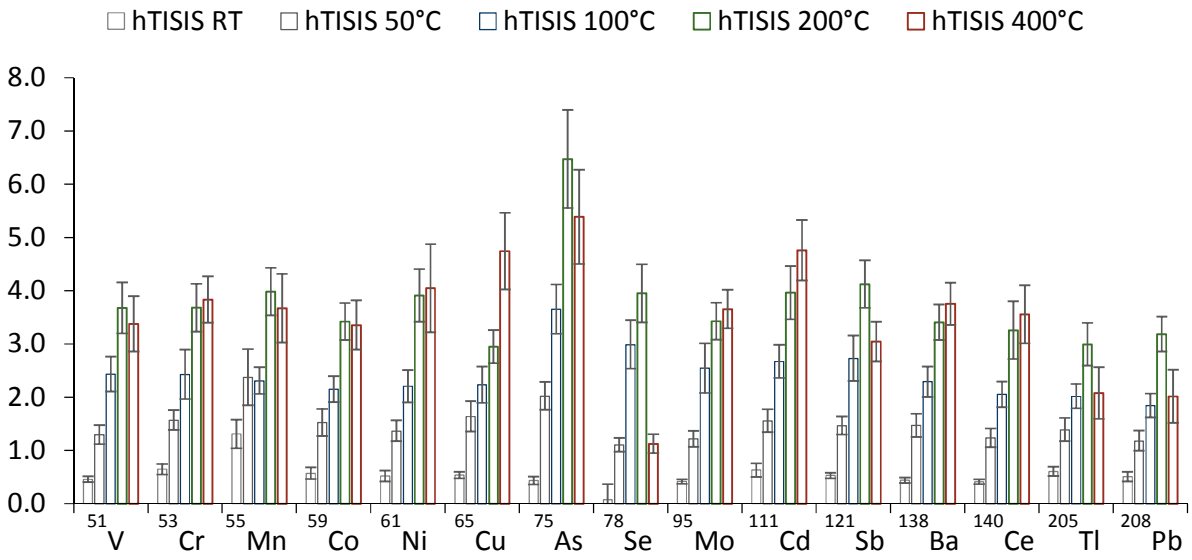

Fig. 1 Effect of the hTISIS temperature on the peak area normalized with respect to the double pass spray chamber. The CSF sample was spiked with 20 µg element L^{-1}. Error bars were calculated according to error propagation (n=5).

View Article Online
DOI: 10.1039/C7JA00210F

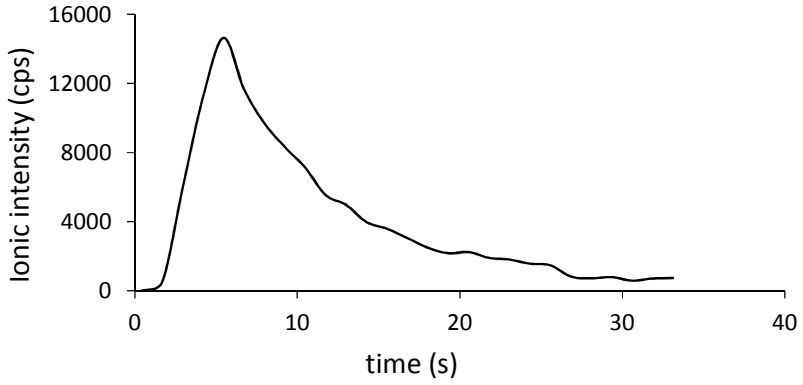

(a)

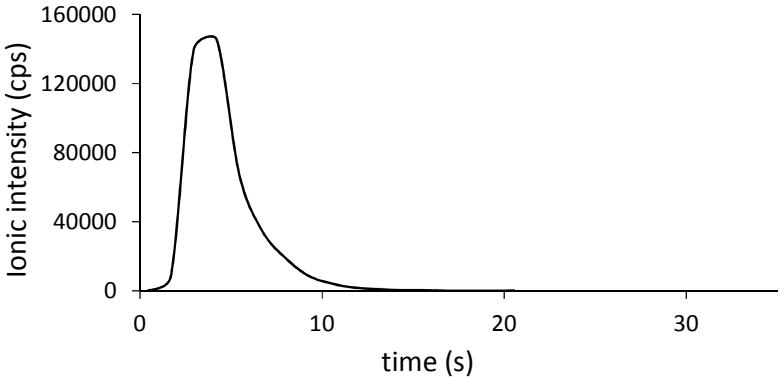

(b)

Fig. 2. ^{51}V transient signals obtained for the double pass spray chamber (a) and the hTISIS operated at 200°C (b). CSF sample was spiked with 20 µg element L^{-1}.

View Article Online
DOI: 10.1039/C7JA00210F

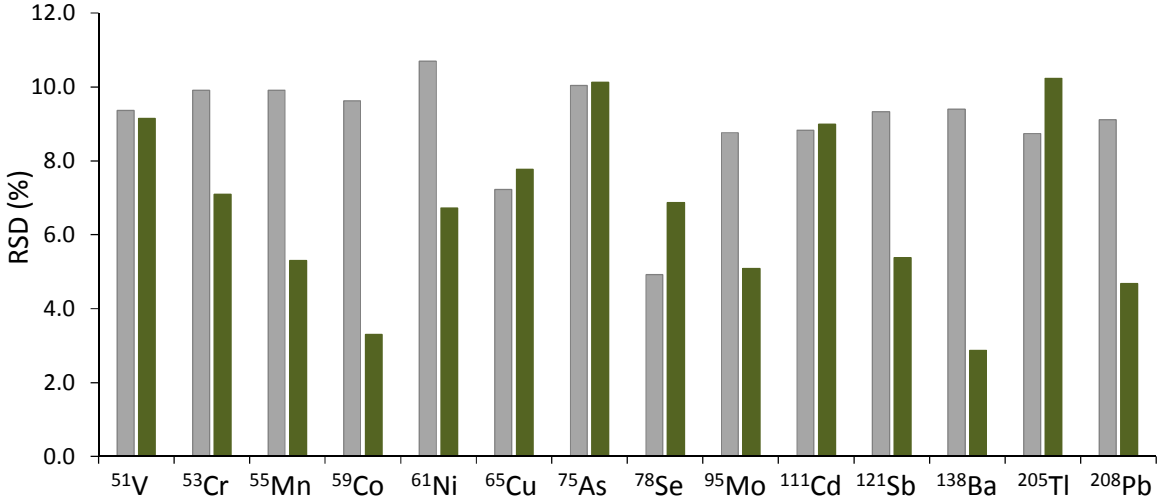

Fig. 3 Peak area RSD (n=5) for the Scott spray chamber and hTISIS at 200°C. Grey bars: Double pass spray chamber; green bars: hTISIS 200°C.

View Article Online
DOI: 10.1039/C7JA00210F

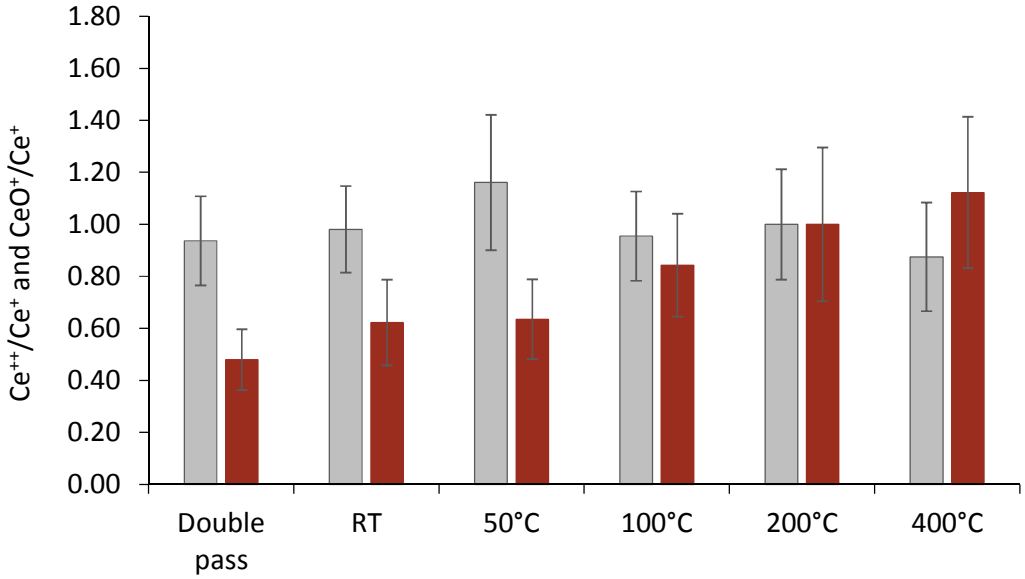

Fig. 4 Variation of cerium oxide (grey bars) and doubly charged ions ratios (red bars) for the hTISIS and the Scott spray chamber normalized with respect to the data found at 200°C. Error bars were calculated according to error propagation (n=5).

View Article Online
DOI: 10.1039/C7JA00210F

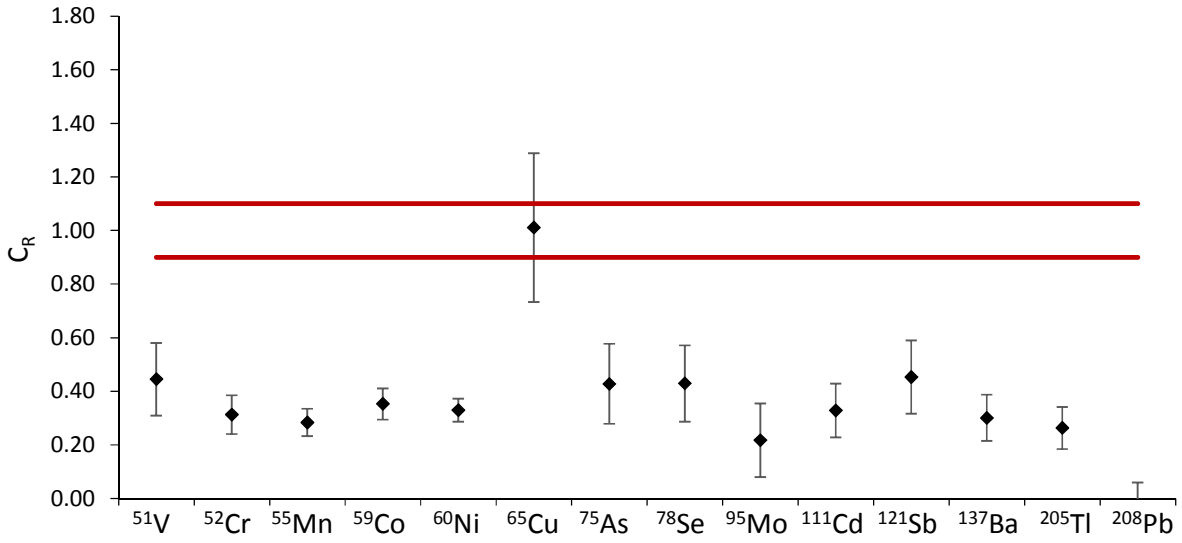

(a)

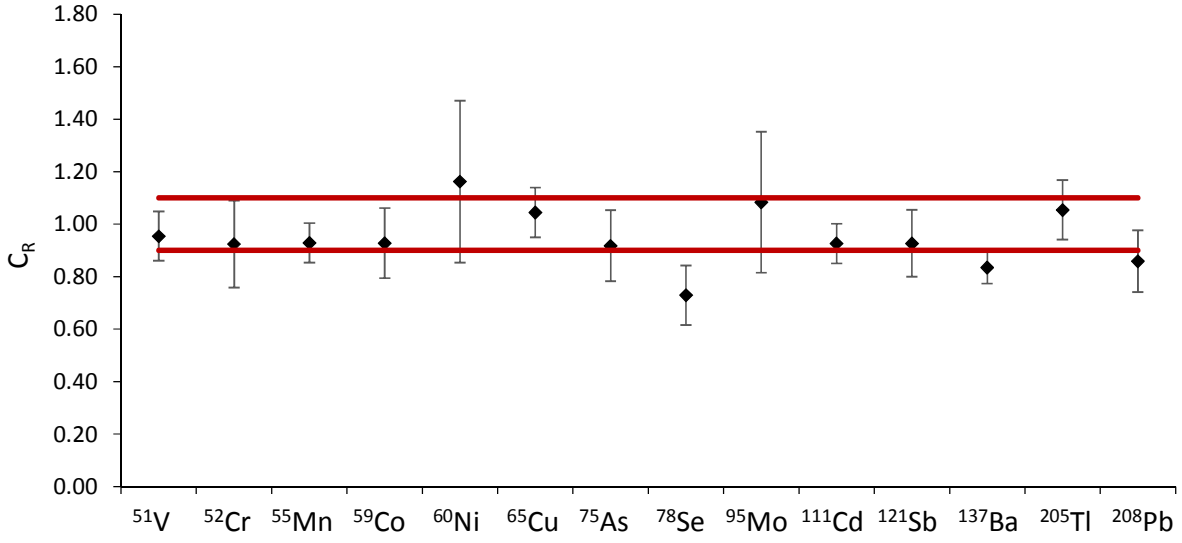

(b)

Fig. 5 Relative elemental concentrations, C_R, obtained for the two calibration methods evaluated. (a) Double pass spray chamber; (b) hTISIS at 200°C. Sample C.

View Article Online
DOI: 10.1039/C7JA00210F

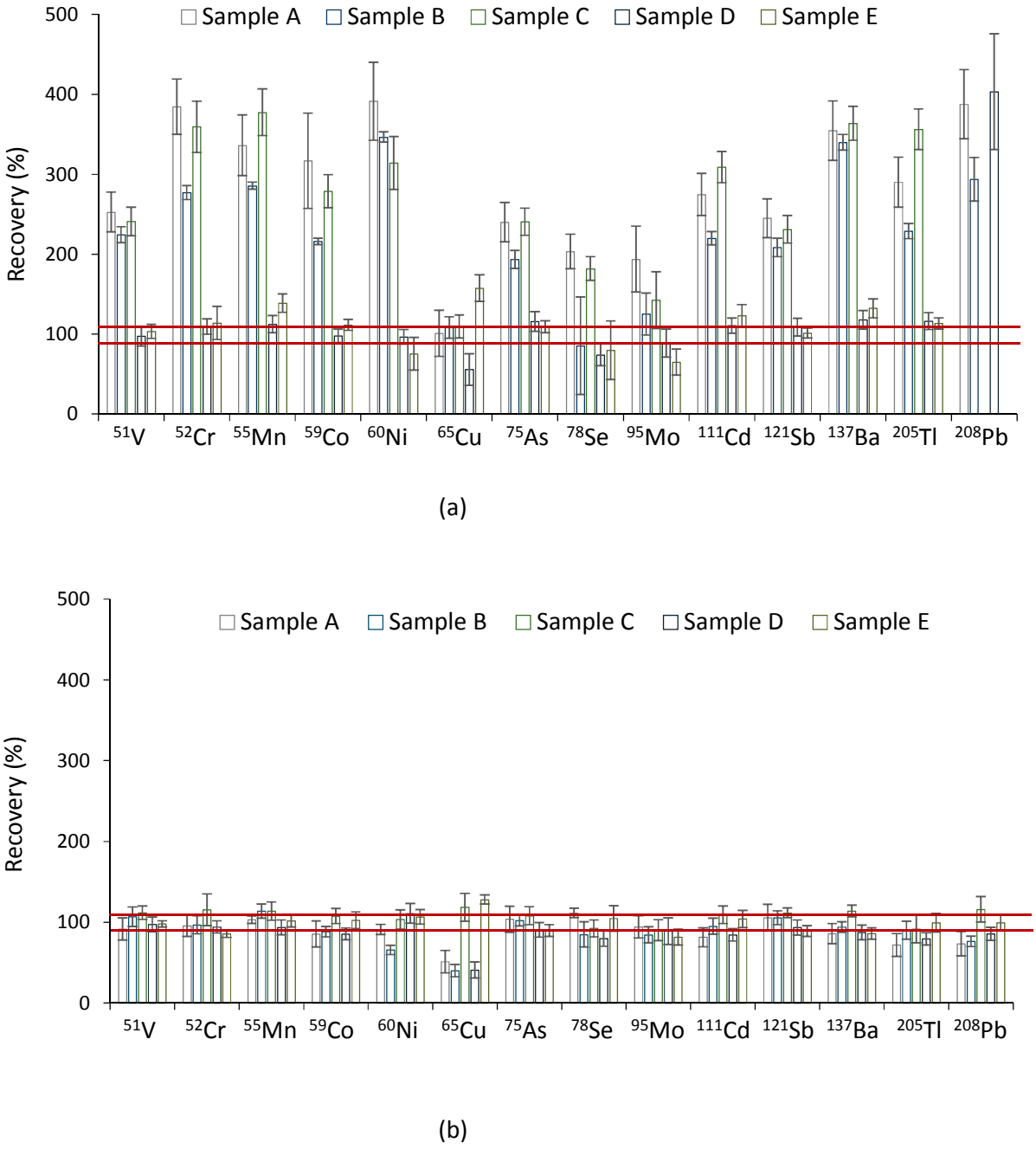

Fig. 6 Recoveries for (a) Scott spray chamber and (b) hTISIS at 200°C for five CSF real samples spiked with 20 µg element L^{-1}.